Supplemental Information:

Hyperbolic Tiling on the Gyroid Membrane in Block Copolymers

Tomonari Dotera

Department of Physics, Kinki University,

Kowakae 3-4-1, Higashi-Osaka 577-8502, Japan

Kenichi Hayashida*, Atsushi Takano, and Yushu Matsushita

Department of Applied Chemistry, Graduate School of Engineering,

Nagoya University, Nagoya 464-8603, Japan

Junichi Matsuzawa

Department of Mathematics, Nara Women's University,

Kitauoyahigashi-machi, Nara 630-8506, Japan

(Dated: January 13, 2011)

* Present Address: Organic Materials Research Lab, Toyota Central R&D Labs., Inc., Nagakute, Aichi 480-1192, Japan.

Contents

I. SAMPLE PREPARATION

Table I summarises the volume ratios of the three components in two ISP star-shaped block polymer samples used in this study together with their molecular weights and molecular weight distributions (MWDs). Three other samples were also obtained by blending the two star polymers as shown in Table I. Their compositions were determined using a 500 MHz ^{1}H NMR spectrometer (Varian Inc., Unity Inova 500). The number-average molecular weight of the common S precursor and the MWDs of the entire polymer samples were determined by SEC calibrated with standard polystyrene samples. These analyses were carried out using an SEC system (Tosoh Ltd.) equipped with a set of three separation columns of 300 mm $\times$ 7.8mm i.d. -G4000$_{\mathrm{HR}}$ and a refractive index detector (RI-8021).

As for SAXS experiments, the wavelength of the X-ray was 0.12 nm, and the size of the X-ray microbeam was approximately 5 μm $\times$ 5 μm (fwhm). The precise camera length was calibrated using a standard collagen sample. For the microbeam SAXS measurements, the annealed sample films were cut into thin sections with a thickness of 30 μm using an ultramicrotome (Reica, Ultracut FCS) with a diamond knife (Diatome, cryo T). These polymer samples were placed on a sample stage and scanned in 1-10 μm steps to look for the crystal planes of the sample parallel to the incident beam.

II. PHASE BEHAVIOUR OF THE ISP STAR-SHAPED BLOCK COPOLYMER

Table II summarises the morphologies formed by the $\mathrm{I}_1\mathrm{S}_{1.8}\mathrm{P}_X$ star-shaped block copolymers, which have been identified in our consecutive works. The shapes of the combined domains made of the I and S components are varied from matrix to gyroid membranes, to lamellae, to cylinders, and to spheres, while those of the P domains are varied from cylinders to gyroidal struts, to lamellae, and to matrix with increasing X. This morphological transition is analogous to that of AB-diblock copolymers.

TABLE I: Characteristics of the ISP Star-Shaped Block Copolymer Samples

Sample	$M_n \times 10^{-3}$	Mw/Mn^a	Formulation (weight fraction)	$\Phi_{\mathrm{I}} : \Phi_{\mathrm{S}} : \Phi_{\mathrm{P}}{}^b$
I precursor	13.3^c	1.04	-	-
S precursor	27.4^a	1.01	-	-
$\mathrm{I_1}$-b-$\mathrm{S_{1.8}}$	40.7^d	1.03	-	1.00 : 1.82 : 0.00
$\mathrm{I_1S_{1.8}P_{3.2}}$	92.1^d	1.02	-	1.00 : 1.83 : 3.17
$\mathrm{I_1S_{1.8}P_{3.5}}$	-	-	$\mathrm{I_1S_{1.8}P_{3.2}/I_1S_{1.8}P_{4.3}}$ (0.657/0.343)	1.00 : 1.83 : 3.49
$\mathrm{I_1S_{1.8}P_{3.8}}$	-	-	$\mathrm{I_1S_{1.8}P_{3.2}/I_1S_{1.8}P_{4.3}}$ (0.329/0.671)	1.00 : 1.83 : 3.84
$\mathrm{I_1S_{1.8}P_{4.0}}$	-	-	$\mathrm{I_1S_{1.8}P_{3.2}/I_1S_{1.8}P_{4.3}}$ (0.200/0.800)	1.00 : 1.83 : 3.99
$\mathrm{I_1S_{1.8}P_{4.3}}$	110^d	1.01	-	1.00 : 1.83 : 4.25

[a]Determined by SEC using polystyrene standard samples.

[b]Volume ratios of I:S:P were calculated using bulk densities of the components, i.e., 0.926, 1.05, and 1.14 g/cm^3 for the I, S, and P components, respectively.

[c]Determined by ^{1}H NMR.

[d]Estimated by ^{1}H NMR based on M_n of the S precursor.

TABLE II: Morphological Transition for the $\mathrm{I_1S_{1.8}P}_X$ Star-Shaped Block Copolymers

X	morphology	combined I and S domain	P domain	$\Phi_{\mathrm{P}}{}^a$
0	cylinder	-	-	0.00
0.8-2.9	tiling-cylinders[b]	matrix	cylinder	0.22-0.51
3.2-3.8	hyperbolic tiling-on-gyroid	membrane	strut	0.53-0.58
4.0-11	cylinders-in-lamella	lamella	lamella	0.59-0.80
12-32	lamellae-in-cylinder	cylinder	matrix	0.81-0.92
53	lamellae-in-sphere	sphere	matrix	0.95

[a]Volume fraction of the P component.

[b]Identified in the previous work for the same $\mathrm{I_1S_{1.8}P}_X$ series.

III. ESCHER'S CIRCLE LIMIT IV AND ARCHIMEDEAN TILING ($3^3.4.3.4$)

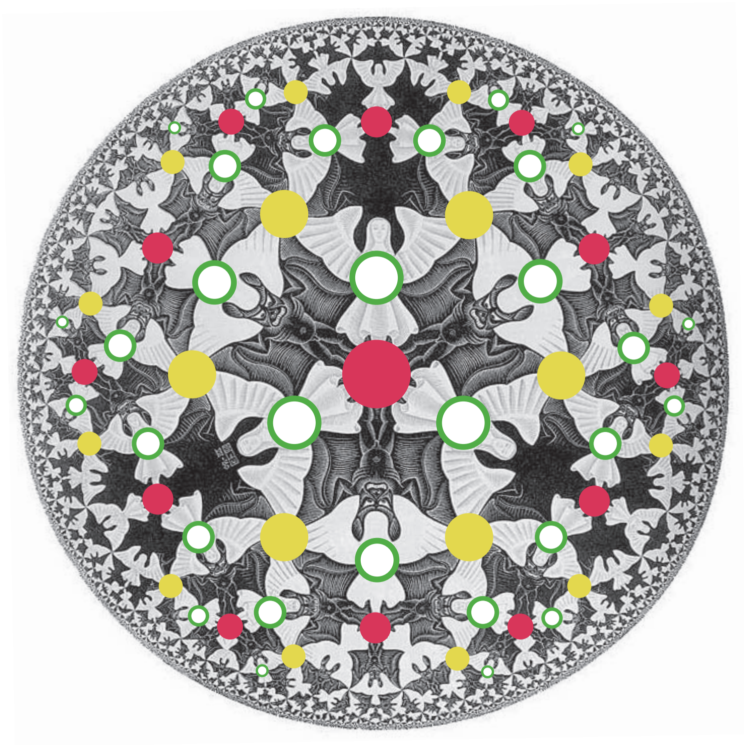

Fig.S 1: Circle Limit IV (Heaven and Hell) superimposed by the hyperbolic Archimedean tiling ($3^3.4.3.4$) vertices (green circles).

IV. SADDLE POINTS OF THE GYROID SURFACE

Site symmetry points, $.\bar{3}.$ and $\bar{4}..$ of space group $Ia\bar{3}d$, are denoted as $16a$ and $24d$, representing multiplicity and Wyckoff letter. Sixteen positions of $16a$ are located at (0,0,0), (1/2,0,1/2), (0,1/2,1/2), (1/2,1/2,0), (3/4,1/4,1/4), (3/4,3/4,3/4), (1/4,1/4,3/4), (1/4,3/4,1/4), and translated ones with (1/2,1/2,1/2). They constitute a BCC lattice with a half lattice constant, and are monkey saddle points as shown in Fig.S2a.

Twenty-four positions of $24d$ are (3/8,0,1/4), (1/8,0,3/4), (1/4,3/8,0), (3/4,1/8,0), (0,1/4,3/8), (0,3/4,1/8), (3/4,5/8,0), (3/4,3/8,1/2), (1/8,1/2,1/4), (7/8,0,1/4), (0,1/4,7/8), (1/2,1/4,1/8), and translated ones with (1/2,1/2,1/2). They are (horse) saddle points of the surface. See Fig.S2b.

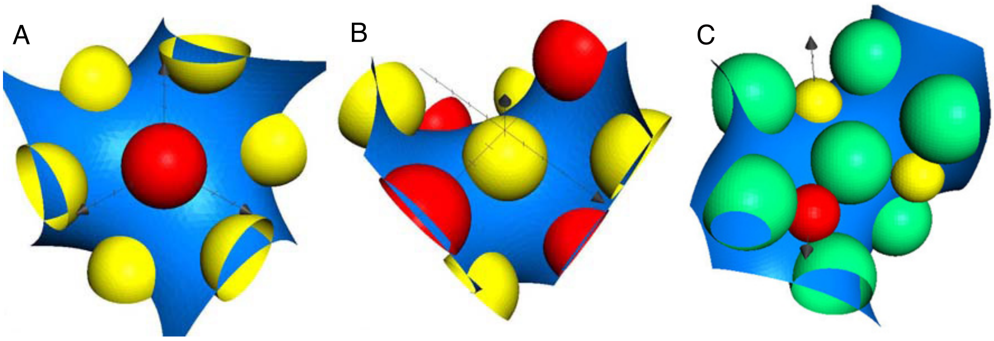

Fig.S 2: **a**, $16a$ (red) and **b**, $24d$ (yellow) positions. G surface is depicted in blue. They are monkey saddle and horse saddle points, respectively. **c**, Vertices (green) of the $(3^3.4.3.4)$ tiling.

V. WEIERSTRASS AND ENNEPER REPRESENTATION

According to Ref.8, the gyroid minimal surface is evaluated by the Weierstrass and Enneper representation:

$$(x, y, z) = \mathrm{Re}\left(e^{i\alpha}\int_0^\omega (1-\omega'^2)R(\omega')\mathrm{d}\omega',\right.$$
$$\left. e^{i\alpha}\int_0^\omega i(1+\omega'^2)R(\omega')\mathrm{d}\omega', e^{i\alpha}\int_0^\omega 2\omega'^2 R(\omega')\mathrm{d}\omega'\right), \tag{S1}$$

where $R(\omega)$ is given by

$$R(\omega) = \frac{1}{\sqrt{1 - 14\omega^4 + \omega^8}}$$

for the P, D, and G triply periodic minimal surfaces. The Bonnet angle for the G surface is exactly written as

$$\alpha = \cot^{-1}\left[\frac{K(\sqrt{3}/2)}{K(1/2)}\right] \fallingdotseq 38.0147^\circ,$$

where $K(x)$ is the complete elliptic integral of the first kind. We calculated these integrals using the incomplete elliptic integrals of the first kind for the shaded region in the complex plane (Fig.S3). Red, yellow and green points in Fig.S4 are mapped to saddle points $16a$ and $24d$ as shown in Fig.S2ab, and to a vertex of the $(3^3.4.3.4)$ tiling on the G surfece, respectively. Applying suitable scaling, rotation and displacement transformations, we could find the coordinates of vertices given in the paper. Note that the values are the same as those obtained by the approximation form

$$\sin 2\pi x \cos 2\pi y + \sin 2\pi y \cos 2\pi z + \sin 2\pi z \cos 2\pi x = 0,$$

up to three digits. The full surface can be easily generated by the symmetry operation of the space group $I\bar{4}3d$.

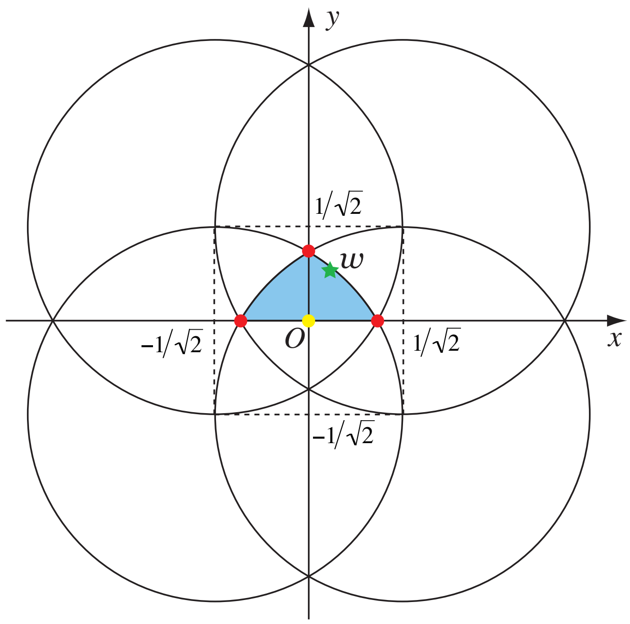

Fig.S 3: The region of ω for the integrals of the Weierstrass and Enneper representation. The blue region is minimal for the space group $I\bar{4}3d$. Red and yellow points are mapped to $16a$ and $24d$ saddle points, respectively. The green star is mapped to a vertex of the $(3^3.4.3.4)$ tiling.

VI. ADDITIONAL RESULTS OF TEM OBSERVATION

A. TEM stained with I_2

We show an image of the [001] projection for the $I_{1.0}S_{1.8}P_{3.2}$ sample demonstrating an interesting symmetry by chance, which provides an additional evidence of the space group. See Fig.S4a. There are left-hand and right-hand windmills located at the centres of squares and the pattern show the plane group $p4gm$. We point out that the centres of squares correspond to 4_1 and 4_3 screw axes of the space group $Ia\bar{3}d$. The lattice constant a is estimated from the relationship; $a = (\sqrt{2} + \sqrt{6})d'/2$, where d' denotes the edge-length of squares. The average value of d' in Fig.S4 gives a lattice constant of ∼90 nm, which agrees with other estimations. TEM simulation perpendicular to the [001] direction is shown in Fig.S4b. The relative contrast was represented by 0.3 for S and I, 1.0 for P in the case of I_2. When the sample is thin enough, say, $0.5a$, and the place is fine-tuned, the simulation reproduces the tiling structure.

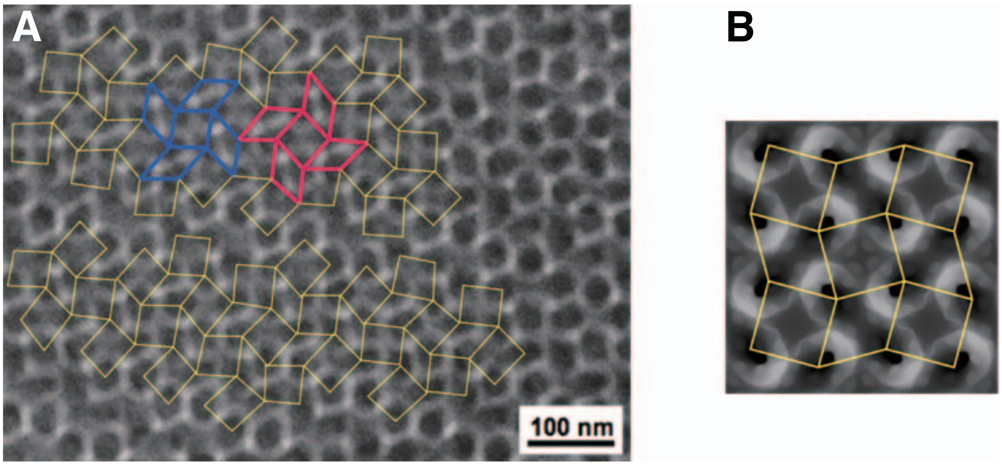

Fig.S 4: **a**, TEM image of the [001] projection for the $I_{1.0}S_{1.8}P_{3.2}$ sample stained with I_2. Two domains of tiling structures with $p4gm$ plane group are superimposed. The centre of a square corresponds to the 4_1 or 4_3 screw axis of $Ia\bar{3}d$. **b**, TEM simulation stained with I_2, perpendicular to [001] for the $(3^3.4.3.4)$ model. The thickness is $0.5a$, and the z-coordinate is from $0.125a$ to $0.625a$, where a is the lattice constant.

B. TEM stained with OsO_4

The osmium tetroxide (OsO_4) stains the I component heavily, thus the shape of I domains are investigated. We find following facts that are the basis of the model structure:

(1) The I component constitute isolated domains as shown in Fig.S5. To check the domains are compact, we show a series of TEM images of the $I_1S_{1.8}P_{3.2}$ sample at the same sample location with different tilt angles. TEM images were taken with a tilt angle range of $-20° \leq \phi \leq 20°$ in 10° steps obtained by inclining the sample stage on a horizontal axis, where the sample was cut into ultrathin sections of 50 nm thickness and stained with OsO_4. As the sample is tilted from -20° to 20°, the black I phase appears to form isolated domains, not to form infinite cylinders, nor networks.

(2) The isolated I domains look prolate (rod-like), but not oblate (disk-like).

(3) The distance between ellipsoids appears to be equal to or greater than 25 nm.

(4) Local square arrangement is observed.

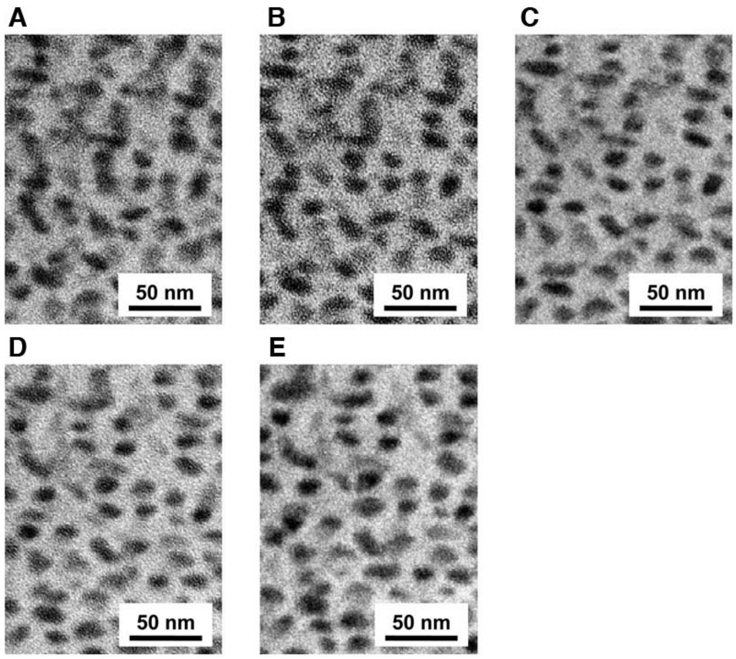

Fig.S 5: TEM images of the $I_1S_{1.8}P_{3.2}$ sample taken with tilt angles of **a**, -20 °, **b**, -10 °, **c**, 0 °, **d**, 10 °, and **e**, 20 ° by inclining the sample around a horizontal axis. The sample was cut into ultrathin sections of about 50 nm thickness and stained with OsO_4.

VII. $(3^6;3^8)$ TILING

Using saddle points shown in Fig.S2, we can construct another hyperbolic tiling $(3^6;3^8)$: all triangles are isosceles and congruent. The numbers of triangle around $16a$ and $24d$ sites are six and eight, respectively. Hence, the tiling can be denoted as $(3^6;3^8)$. We note that these isosceles triangles are close to equilateral triangles: The distance between the nearest $16a$ and $24d$ is $\sqrt{5}/8 = 0.280$, and that between the nearest $24d$ and $24d$ is $\sqrt{6}/8 = 0.306$ in the unit of the lattice constant.

Model Structure from $(3^6;3^8)$: We assume that the I domains are ellipsoidal shapes (prolate spheroid) with $a = b < c$ and $c/a = 1.3$. Major axes are set to be perpendicular to the G surface. Our choices are $a = 0.0914$ and $c = 0.1188$ for $(3^6;3^8)$. For $(3^6;3^8)$, although $16a$ and $24d$ sites are not in the same environment, we assume I domains are the same shape and sizes. Since the lattice constant is 100 nm, the diameters are about 15-25 nm. A three-dimensionally continuous S domain is represented by

$$|\sin 2\pi x \cos 2\pi y + \sin 2\pi y \cos 2\pi z + \sin 2\pi z \cos 2\pi x| < d,$$

except for I domains. We take $d = 0.667$ for $(3^6;3^8)$.

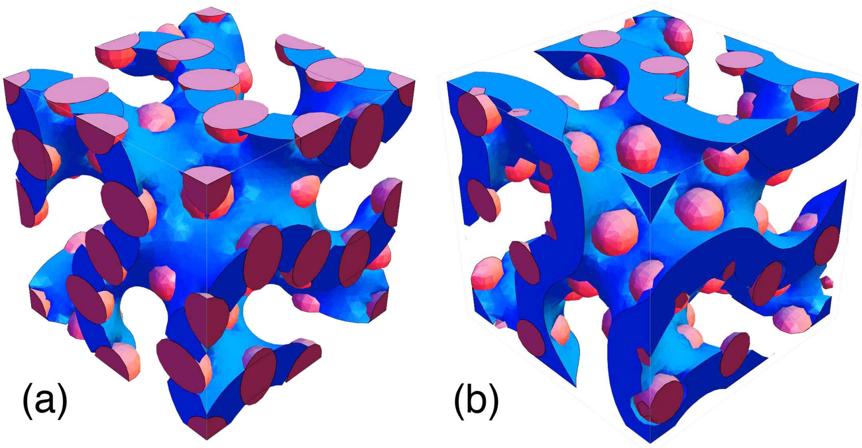

Fig.S 6: Model structures of hyperbolic tiling structure on the G surface: (a) $(3^6;3^8)$ and (b) $(3^3.4.3.4)$ for $I_1S_{1.8}P_{3.2}$. The I component in red and the S component in blue are shown. Remaining transparent double networks are the P component.